High Precision Multiple Parameter Measurement Sensor Based on Constitutive Parameters Near-Zero Media

Qiao Yu Li[1], Yu Wei Mao[1], and Yong Jin Zhou[1,2]

[1]Shanghai Collaborative Innovation Center of Intelligent Sensing Chip Technology
Laboratory of Specialty Fiber Optics and Optical Access Networks, Shanghai University, Shanghai 200444, China
20802117@shu.edu.cn, maoyuwei@shu.edu.cn

[2]State Key Laboratory of Millimeter Waves
School of Information Science and Engineering, Southeast University, Nanjing 210096, China
yjzhou@shu.edu.cn

Abstract **–** A high-precision multiple parameter measurement sensor based on constitutive parameters near-zero (CPNZ) media has been proposed, which can effectively and accurately predict changes in temperature and relative humidity simultaneously and independently. The dual-channel microwave sensor is composed of a double doping CPNZ substrate integrated waveguide (SIW) cavity, which has the capability to predict different parameters independently. A multi-input and multi-output model is constructed to improve the measurement accuracy by training back propagation (BP) neural network. The relative error of the predicted temperature is smaller than 1.3%, with mean square error (MSE) of ± 0.15. The relative error of the predicted relative humidity is smaller than 8.74%, with MSE of ± 0.1. The multiple parameter sensor based on CPNZ materials offers a promising platform for multiple parameter sensing research, providing essential technical support and infrastructure for the development of fields like the Internet of Things, intelligent manufacturing, and smart cities.

Index Terms **–** BP neural network, constitutive parameters near-zero media, high precision, microwave sensor, multiple parameter measurement.

I. INTRODUCTION

Sensors have found wide application across various industries [1–3], healthcare [4–5], automobiles [6–7], aerospace [8–9], and other fields. Traditional sensors suffer from a limitation as they can only measure specific physical quantities, such as temperature [10–11], humidity [12–14], or pressure [15–16]. In scenarios where multiple parameters need measurement, employing multiple sensors in conjunction becomes necessary [17–18]. This not only compromises measurement accuracy but also significantly increases system complexity and measurement costs, leading to an underutilization of sensor functionalities and benefits. Multiple parameter sensors offer a solution by simultaneously measuring multiple different physical quantities, leading to accurate, comprehensive, and cost-effective measurements. They reduce testing costs and time, facilitating automated data collection and analysis. Furthermore, the advancement of multiple parameter sensors has provided essential technical support and infrastructure for the development of fields like the Internet of Things, intelligent manufacturing, and smart cities.

One approach to achieve multiple parameter sensing involves using multiple resonators [19]. These sensors exhibit high accuracy. However, the system is complex and large. Another approach is to use multiple physical quantities (i.e. resonant frequency shift, quality factor) of a single resonator to detect multiple parameters simultaneously [20]. However, non-negligible coupling between the multiple parameters results in limited measurement accuracy and measurement range [19–20]. Therefore, conducting further research on multiple parameter sensors that offer high precision, independent and real-time measurement, integration, and low costs is of significant importance.

Microwave measurement technology has gained prominence in the field of complex permittivity measurement due to its advantages, such as high integration, measurement accuracy, and real-time performance [21]. One example of this is the use of a resonant sensor based on the improved complementary split ring resonator (CSRR) to simultaneously measure changes in complex dielectric constant and complex permeability [22]. To ensure reliable results in scientific research and production, achieving the necessary measurement accuracy is essential in various microwave measurement technologies. Metamaterials, which are artificial electromagnetic structures composed of subwavelength

Submitted On: October 31, 2023
Accepted On: September 2, 2024

https://doi.org/10.13052/2024.ACES.J.390804

resonators, exhibit novel electromagnetic characteristics and find applications in sensing, antennas, stealth technology, and other fields [23–25]. Constitutive parameters near-zero medium, including relative permittivity near-zero and relative permeability near-zero media, has unique electromagnetic control characteristics and is utilized in material characterization, sensors and other fields [26–29]. Such media has been used in high sensitivity sensors, with its field enhancement property. For instance, a double-layer relative permeability near-zero media sensor composed of microstrip lines and metal strips with metal through-holes has been employed for testing magnetic dielectric materials. Although this sensor exhibits minimal measurement error, it suffers from positioning errors that significantly impact measurement of the relative dielectric constant of the sample [29]. Additionally, the substrate-integrated (SI) photon doping method enables the realization of near-zero medium in printed circuit design, providing potential applications in material characterization and sensing [30]. Metamaterials also provide a broad platform for studying relative permittivity near-zero media [31]. For example, a multi-tunnel relative permittivity near-zero media based substrate integrated waveguide (SIW) cavity coupled with a conical microstrip line forms a dual tunnel sensor that demonstrates more than 95% accuracy in measuring dielectric constants of radome, flat substrate, and building materials [31]. Previous sensors are based on relative permittivity near-zero or relative permeability near-zero media. Constitutive parameters near-zero (CPNZ) medium is a special medium with an equivalent relative permeability of zero for the entire structure, which uses relative permittivity near-zero material as the host medium and non-magnetic medium as doping. Since sensors based on CPNZ materials possess superior sensing characteristics, exploring and developing multiple parameter sensors based on CPNZ materials hold promising prospects in the field of sensing technology.

In this paper, the study focused on the theoretical research of multiple parameter CPNZ media and introduced a high-precision dual-channel microwave sensor. The sensor is designed to address scenarios where multiple parameters change independently at the same time. To verify its dominant performance, an experiment is conducted, which is based on the fundamental principles that temperature changes with the relative permittivity of distilled water [26] and relative humidity changes with the relative permittivity of polyimide materials [27]. A neural network is introduced to the multiple-input multiple-output sensor to improve the accuracy of measuring environmental temperature and relative humidity. The obtained results clearly demonstrate that the multiple parameter CPNZ medium sensor effectively and accurately predicts both temperature and humidity of the environment concurrently. These findings highlight the potential of a sensor for practical applications in various fields where multiple parameters need to be measured with high precision and independence.

II. THEORY OF CPNZ MEDIA SENSOR

A. Sensor performance improvement based on CPNZ media

The field enhancement property of near-zero media is highly sensitive to small changes in the material, enabling the measurement of the complex dielectric constant of material. The measurement principle based on near-zero medium is studied below for the first time. According to the basic principle of near-zero medium [32], the relationship between the magnetic field $H_z(\vec{r})$ in the doping and the magnetic field H_z^{ENZ} in the relative permittivity near-zero medium is:

$$H_z(\vec{r}) = H_z^{ENZ}\psi^d(\vec{r}), \tag{1}$$

where $\psi^d(\vec{r})$ is the solution of the scalar Helmholtz equation, reflecting the proportional relationship between the doped internal field and the relative permittivity near-zero medium midfield. By solving the scalar Helmholtz equation [31]:

$$\psi^d(\vec{r}) = \frac{J_0(k_d r)}{J_0(k_d r_d)}, (0 \le r \le r_d). \tag{2}$$

Here J_0represents the first class of zero-order cylindrical Bessel functions and k_d is the wave number in the doped medium.

It can be seen from equation (2) that the field inside the doped medium fluctuates and reaches its strongest at the central point ($r = 0$), that is, the convergence of the magnetic field is reflected at this point [32]. Equation (2) can effectively calculate the enhancement effect of the incident field in the embedded medium in the structure. The integral of the tangential component of the external radiated electric field of the relative permittivity near-zero structure along the edge loop of the relative permittivity near-zero medium is equal to the total magnetic flux of the entire structure cross-section [32]. When the tangential electric field at the edge of the relative permittivity near-zero medium is large, it results in a significant total magnetic flux in the entire structure cross-section, leading to an effective internal magnetic field enhancement effect.

By designing the size of the doping material reasonably, the relative permeability of the original host medium is modified while ensuring the relative permittivity is close to zero. What is more important, the port impedance of the CPNZ structure based on the relative permittivity near-zero media matches the free-space impedance, ensuring that the field of the CPNZ is consistent with the external radiation field. As a result, 100% transmission can be achieved, regardless of the area of the CPNZ region, as long as the width of the incident

and exit ports of the waveguide is the same. Therefore, sensors based on CPNZ materials exhibit both excellent sensing performance and industrial applicability.

B. Multiple parameter sensor based CPNZ media

When doping is added to the relative permittivity near-zero medium, the cross-sectional area of each doping changes. The relative permittivity near-zero background is unchanged, and the equivalent relative dielectric constant is not affected. The equivalent permeability of the host is regulated by a single or multiple doping, with each doping causing a change in the permeability. The response of the relative permittivity near-zero cavity loaded with double doping is analyzed when dielectric cylinders with the same relative permittivity of ε_{rd} and radius of r_s are selected as dopants in this paper. The formula of equivalent relative permeability can be obtained as follows:

$$\mu_{r\_eff} = 1 + \sum_{\mathrm{d}=1}^{\mathrm{n}} \frac{A_d}{A}\left[\frac{2}{k_d r_s}\frac{J_1(k_d r_s)}{J_0(k_d r_s)} - 1\right], \quad (3)$$

where A_d is the cross-sectional area of the different doping medium, A is the cross-sectional area of the relative permittivity near-zero medium, $k_d{=}\varepsilon_{rd}(\omega/c)^2$, and c is the propagation velocity in vacuum.

According to the special solution of the first kind of Bessel function, equation (3) can be simplified to:

$$\bar{\mu}_{r\_eff} = 1 + \sum_{d=1}^{n} \frac{A_d}{A}\left[2\left(\frac{1}{4} + \frac{1}{4-(k_d r_s)^2}\right) - 1\right]. \quad (4)$$

Here,$\overline{\mu}_{eff}$ is the approximate value of μ_{eff}. Substituting k_d into equation (4):

$$\bar{\mu}_{r\_eff} = 1 + \sum_{d=1}^{n} \frac{A_d}{A}\left[\frac{4c^2}{\omega^2 r_s{}^2 \varepsilon_{rd}} - \frac{1}{2}\right]. \quad (5)$$

For the multiple doping relative permittivity near-zero structure, the resonant phenomenon can be seen when $J_0(k_d r_s){=}0$ [32] in equations (4) and (5), as long as each doping can meet the resonant requirements $k_d r_s{=}(\frac{\omega}{c})^2 \varepsilon_{rd} r_s \approx 2\sqrt{2}$ in the paper. For multi-doped relative permittivity near-zero media, the dielectric constants of doping are different, but the corresponding resonant frequencies are different when each doping meets the resonant conditions. It can be demonstrated that the resonances of the two channels are only related to parameters ε_{rd} and r_s, that is, there is no coupling between the two frequencies. A multi-parameter CPNZ sensor is designed based on the characteristics that each channel of multi-doped relative permittivity near-zero medium does not affect each other.

III. DESIGN AND SIMULATION OF CPNZ SENSOR

A. Multiple parameter CPNZ sensor

In order to verify the rationality of multi-parameter sensors based on CPNZ, a double-doped CPNZ materials structure is first designed. The dimensions of the relative permittivity near-zero cavity h=5 mm, l=80 mm are set, and its calculated theoretical cut-off frequency f_p is 5.45 GHz. The double doping CPNZ medium sensor is designed when equation (1) is equal to zero. The relative permittivity of the two doped cylinder ε_{rd} is 92 and radius r_s is set to 2.33 mm. Furthermore, the CPNZ cavity is simulated by a rectangular air waveguide operating near the cutoff frequency of the TE_{10} mode. Figure 1 (a) is the three-dimensional structural diagram of the proposed dual-doped CPNZ medium microwave sensor, which combines the rectangular air waveguide and two SIW cavities. The dielectric substrate of the sensor is F4B, its relative permittivity is 2.65, and loss tangent is 0.002. The length L of the whole structure is 213 mm, width W is 35.6 mm, and height h is 5 mm. The rectangular air waveguide is the CPNZ body and its length l is set to 80 mm and width w is 27.5 mm. The two SIW cavities are introduced as excitation for the CPNZ body to achieve normal propagation of electromagnetic waves. Figures 1 (b) and (c) show top view and side view of the CPNZ sensor. The sensor is excited by coaxial line, where the inner conductor of the coaxial line is embedded inside the SIW cavity. The excitation position is indicated by the dashed line in Figs. 1 (a) and (b).

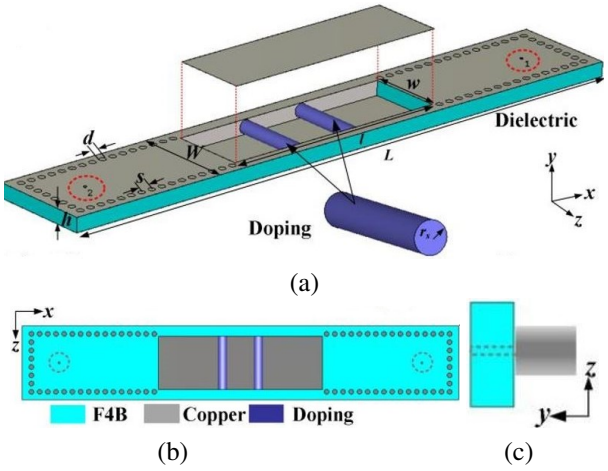

Fig. 1. (a) Structural diagram, (b) top view, and (c) side view of double-doped CPNZ media sensor.

Figure 2 (a) shows the transmission coefficients of the CPNZ structure, and it can be seen that its resonant frequency is 5.45 GHz which is coincident with the theory frequency. The electric and magnetic field distributions of the CPNZ structure at 5.45 GHz are shown in Fig. 2 (b). It can be seen that the electric field is mainly concentrated on the edge of the doped cylinder, while the magnetic field is mainly concentrated on the inside of the doped cylinder. Such field enhancement will lead to high sensitivity of the sensor to small changes in ambient dielectric change. Figure 2 (c) shows the magnetic field

phase distribution. The magnetic field phase distribution is uniform at the resonant frequency, that is, the equivalent relative permittivity and equivalent relative permeability of the doped CPNZ cavity are both zero, which is the medium characteristics of CPNZ [32].

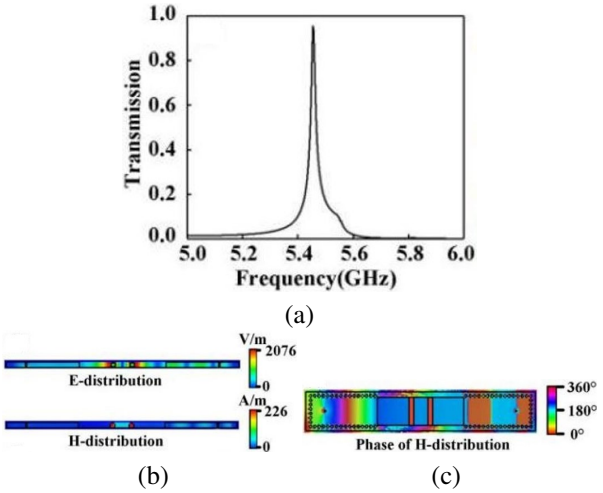

Fig. 2. Double-doped CPNZ media sensor: (a) transmission coefficients, (b) electric field distribution and magnetic field distribution at 5.45 GHz, and (c) magnetic field phase distribution at 5.45 GHz.

To achieve simultaneous measurement of multiple parameters, the double-doped sensor has been improved. Firstly, two cylinders are hollowed out and doped in the middle, and then two holes are etched on both sides of the medium substrate to facilitate the placement of the materials to be tested later. The improved dual-channel sensor structure is depicted in Fig. 3 (a). Due to processing technology limitations, a wall thickness of 0.33 mm is selected. The transmission coefficient of the dual-channel sensor without any material loaded is shown in Fig. 3 (b), where a transmission peak at 5.1 GHz is observed. The frequency change of transmission coefficient is determined by a combination of the doped area and the doped dielectric constant. After digging holes, the cross-sectional area of doping A_d becomes smaller, leading to a reduction in the equivalent permeability. In this case, the effect of area change is greater than the effect of equivalent dielectric constant, resulting in a red-shifted frequency after hollowing out the doping material. The electric field mainly concentrates on the edges of the two doped cylinders, while the magnetic field mainly concentrates on the interior of the cylinders, as shown in Fig. 3 (c). The local concentration of electric and magnetic fields is conducive to the ability of the sensor to detect multiple parameters simultaneously.

From equation (3), it is evident that when the two dopings have the same shape but different equivalent

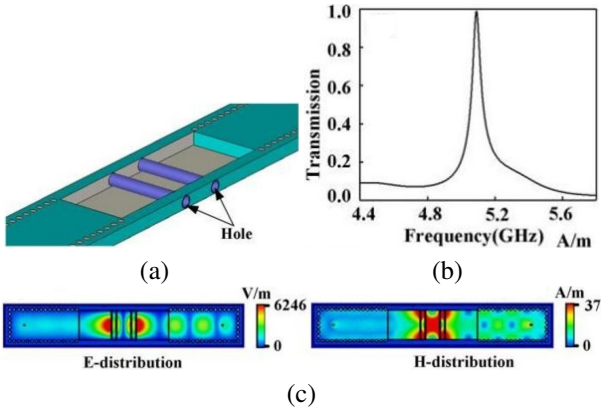

Fig. 3. (a) Structural diagram of a two-channel sensor (the upper metal is hidden), (b) transmission coefficients S_{21}, and (c) electric field distribution and magnetic field distribution at 5.1 GHz.

dielectric constants, two resonant points with distinct resonant frequencies will emerge. To verify this, two cylindrical channels were filled with polyimide material and distilled water, respectively, as illustrated in Fig. 4 (a). The transmission coefficients generate two resonant frequency points at 4.74 GHz and 5.75 GHz, as shown in Fig. 4 (b). The resonant frequency point at 4.74 GHz corresponds to the channel filled with polyimide material. Similarly, the resonant frequency point at 5.75 GHz corresponds to the channel filled with distilled water. The electric field distribution at the two resonant frequency points is presented in Fig. 4 (c). It is evident that the two channels do not influence each other significantly. At 4.74 GHz, the electric field in the channel filled with polyimide material is the strongest, whereas at 5.75 GHz, the electric field in the channel filled with distilled water is the strongest. As a result, the two resonant points remain independent of each other, which is

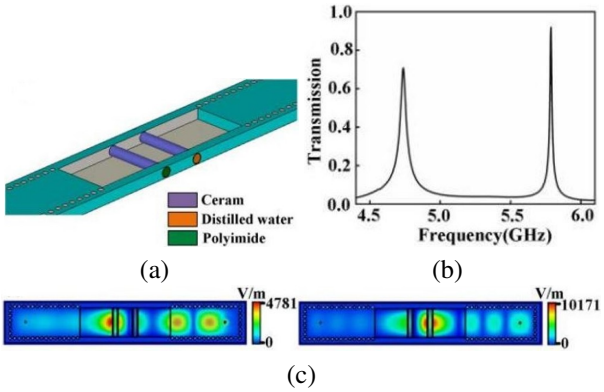

Fig. 4. (a) Dual-channel sensor loaded with polyimide material and distilled water, (b) transmission coefficients S_{21}, and (c) electric field distribution maps corresponding to 4.74 GHz and 5.75 GHz.

advantageous for accurately measuring ambient temperature and relative humidity without interference.

B. Sensor simulation data acquisition

The detection principle of the temperature and humidity sensor relies on the fact that the relative permittivity of polyimide material changes with relative humidity and the relative permittivity of distilled water changes with temperature. During normal operation of the power system, national regulations for power capacitors generally set the ambient temperature limit at 40℃. Therefore, an environment temperature of 35℃ is assumed. At this temperature, the relative permittivity of distilled water remains constant, while the relative humidity of the environment is varied. The relative permittivity of polyimide materials is systematically increased from 2 to 4.5 with a step value of 0.1 (total 26 sets). Transmission coefficients are shown in Fig. 5 (a). It can be observed that the second resonant point almost remains unchanged, while the first resonant point experiences a red-shift with increasing relative permittivity of the polyimide material. Next, an ambient relative humidity of 68% is set and the relative permittivity of the polyimide material constant is kept. The relative permittivity of distilled water is increased from 60 to 74 with a step value of 1 (total 15 sets). The corresponding transmission coefficients are shown in Fig. 5 (b). The first resonant frequency point almost remains unchanged, while the second resonant frequency point red-shifts with the increase in the relative permittivity of distilled water. From the above results, it can be seen that the dual-channel CPNZ media sensor can effectively detect changes in temperature and relative humidity, respectively, by varying the relative permittivity of the polyimide material or distilled water. This phenomenon also corresponds to the theory, that is, two channels without significant interference.

Changing the relative permittivity of polyimide and distilled water simultaneously, we obtained a total of 26×15=390 sets of transmission coefficient data by simulation. Parts of the corresponding transmission coefficients are depicted in Fig. 6. It is shown that the resonant frequency point experiences a red-shift with an increase in the relative permittivity of the polyimide material. Similarly, the second resonant frequency point also red-shifts with an increase in the relative permittivity of the distilled water. This observation confirms that the sensor is capable of simultaneously measuring temperature and relative humidity of the environment. In conclusion, the dual-channel CPNZ media sensor demonstrates its ability to accurately measure both temperature and relative humidity when subjected to changes in both parameters. The red-shift of the resonant frequency points in Fig. 6 validates the capability of the sensor for multi-parameter measurement, making it a promising solution for environmental monitoring and other applications.

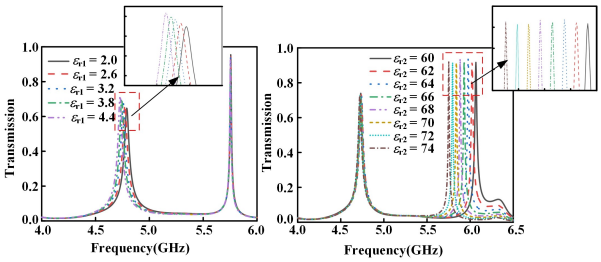

(a) (b)

Fig. 5. (a) Transmission coefficients corresponding to the relative permittivity of different polyimide materials and (b) transmission coefficients corresponding to the relative permittivity of different distilled waters.

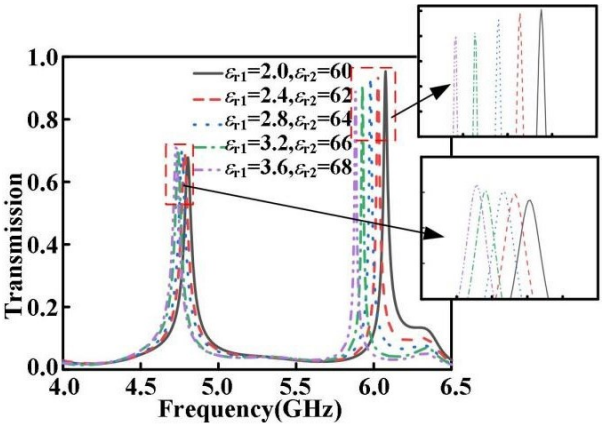

Fig. 6. Transmission coefficients corresponding to the relative permittivity of distilled water and polyimide materials.

C. Parameter inversion based on neural network

Neural networks have proven to be effective data processing tools in the microwave field due to their strong nonlinear fitting capabilities. Polyimide materials and distilled water data are obtained from the simulation of the S parameter of relative permittivity. To determine the temperature and relative humidity of the environment, an inverse problem needed to be solved. Considering the presence of multiple independent variables and dependent variables, the authors used back propagation (BP) neural networks as the data processing tool to build a multiple-input multiple-output model, thus improving the accuracy of measuring environmental temperature and relative humidity [33].

The obtained sample data were used to train the BP neural network and establish the required inversion model. The structure of the BP neural network is illustrated in Fig. 7, where the first resonant frequency f_1

and the second resonant frequency f_2 from the transmission curve serve as input data, while the output data consisted of temperature and relative humidity of the environment in which the sensor was located. By employing the BP neural network and training it with the sample data, the researchers were able to create a model that accurately predicts the environmental temperature and relative humidity based on the input resonant frequencies. The multiple-input multiple-output approach of the neural network allowed for efficient handling of the complex relationships between the input and output variables, ultimately leading to improved measurement accuracy for environmental monitoring in the microwave field.

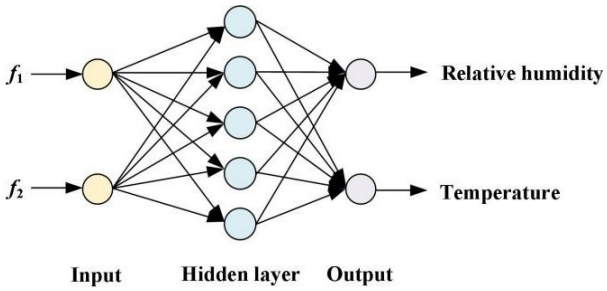

Fig. 7. Structural diagram of BP neural network.

On the basis of 390 sets of S parameters obtained by simulation of a dual-channel CPNZ media sensor, a BP neural network is used to establish the relationship between the first resonant frequency f_1, the second resonant frequency f_2, temperature and relative humidity, and inversion. The comparison between the predicted value and the expected value of the training set is shown in Fig. 8 (a). The results show that the predicted value is in great agreement with the actual value. In the figure, mean square error (MSE) represents the expected value of the squared difference between the predicted value and the actual value, and its calculation equation is:

$$MSE = \frac{1}{n}\sum_{i=1}^{n}(y_i - \hat{y}_i)^2. \tag{6}$$

The smaller the value of MSE, the better the ability of the model to fit the experimental data. Figure 8 (b) shows MSE values of different temperature and relative humidity in the training set. Results show that MSE values between the predicted value and the actual value of the BP neural network model for temperature and relative humidity are within ± 0.8. The coefficient of determination of temperature prediction model is 0.94629, and the coefficient of determination of relative humidity prediction model is 0.99711, indicating that the two prediction models have a good degree of fit.

In order to verify the accuracy of the model obtained by the BP neural network in measuring ambient temperature and relative humidity, five groups of different environmental conditions are set: relative humidity is 25% and temperature is 45℃; relative humidity is 30% and temperature is 50℃; relative humidity is 35% and temperature is 55℃; relative humidity is 40% and temperature is 60℃; and relative humidity is 45% and temperature is 65℃.

The resonant frequencies of these five groups of test data are extracted and inverted by the model. Comparison between the predicted value and the expected value and the distribution of MSE are shown in Figs. 9 (a) and (b). As can be seen from Fig. 9 (a), the predicted value is in good agreement with the expected value. It can be seen from Fig. 9 (b) that the MSE value of temperature is ± 0.15 and that of relative humidity is ± 0.1, indicating that the model obtained by using BP neural network training sample data has good measurement accuracy for ambient temperature and relative humidity.

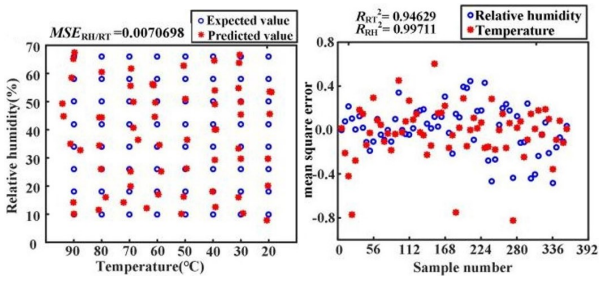

Fig. 8. (a) Comparison of predicted value and expected value of the training set and (b) MSE value of the training set.

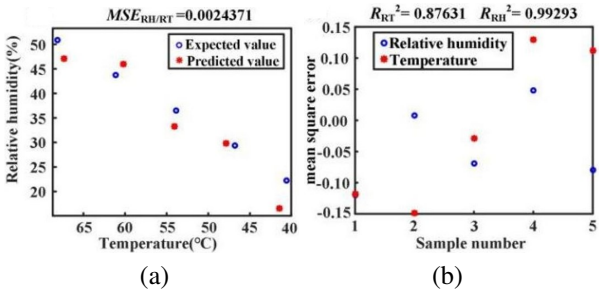

Fig. 9. (a) Comparison of predicted value and expected value of the test set and (b) MSE value of the test set.

Table 1 summarizes the performance comparison of the proposed sensor and other state-of-the-art multi-parameter measurement sensors. Multiple parameters were obtained by using two modes generated by one sensor in reference [20]. However, the two modes cannot be independently regulated.

Table 1: Performance comparison of multi-parameter measurement sensors.

Ref.	Independent	Relative Error (f_1)	Relative Error (f_2)
[20]	No	TH<4.86%	ε'<0.1% ε''<2.3%
[34]	Yes	ε'<1.5% ε''<6.67%	ε'<2.8% ε''<6.25%
[35]	Yes	μ_r<1.81%	μ_r<8%
[36]	No	ε'<10%	ε'<10%
[37]	Yes	ε'<5%	ε'<5%
[38]	Yes	T<2.33%	RH<9%
This work	Yes	T<1.3%	RH<8.74%

Thickness (TH), real part of the dielectric constant (ε'), imaginary part of the dielectric constant (ε''), relative permeability (μ_r), temperature (T), relative humidity (RH)

Sensors in references [34–38] measure different physical quantities by using multiple sensors, which leads to a large system volume and difficult integration. The operating resonant frequencies of the proposed sensor are independent of each other, and measure the temperature and relative humidity simultaneously without influencing each other. Relative errors of the predicted temperature and relative humidity are smaller than 1.3% and 8.74%, respectively.

IV. CONCLUSION

Based on theoretical analysis of double doping, this paper proposes a high precision CPNZ medium microwave sensor for multi-parameter measurement. Results show that the two-channel CPNZ media sensor does not exhibit coupling effects between the two operating frequencies. By training the BP neural network, a multi-input multi-output model is constructed to improve measurement accuracy. From the testing results of five groups of different environmental conditions, relative errors of the predicted temperature and relative humidity are smaller than 1.3% and 8.74%, respectively, indicating the sensor's high measurement accuracy and its ability to monitor changes in multiple parameters simultaneously.

ACKNOWLEDGMENT

This work is supported by the National Natural Science Foundation of China under Grant No. 61971469 and Fundamental Research Funds of Shaanxi Key Laboratory of Artificially-Structured Functional Materials and Devices (AFMD-KFJJ-21105).

REFERENCES

[1] J. Riegel, H. Neumann, and H. M. Wiedenmann, "Exhaust gas sensors for automotive emission control," *Solid State Ionics*, vol. 152, pp. 783-800, Mar. 2002.

[2] Y. Liu, Y. Yang, X. P. Lv, and L. F. Wang, "A self-learning sensor fault detection framework for industry monitoring IoT," *Math. Probl. Eng.*, vol. 2013, pp. 1-8, Jan. 2013.

[3] M. Y. Aalsalem, W. Z. Khan, W. Gharibi, M. K. Khan, and Q. Arshad, "Wireless sensor networks in oil and gas industry: Recent advances, taxonomy, requirements, and open challenges," *J. Netw. Compu. Appl.*, vol. 113, pp. 87-97, July 2018.

[4] K. Yeshwant and R. Ghaffari, "A biodegradable wireless blood-flow sensor," *Nat. Biomed. Eng*., vol. 3, no. 1, pp. 7-8, Jan. 2019.

[5] C. M. Boutry, L. Beker, Y. Kaizawa, C. Vassos, H. Tran, A. C. Hinckley, R. Pfattner, S. Niu, J. Li, J. Claverie, Z. Wang, J. Chang, P. M. Fox, and Z. Bao, "Biodegradable and flexible arterial-pulse sensor for the wireless monitoring of blood flow," *Nat. Biomed. Eng*., vol. 3, pp. 47-57, Jan. 2019.

[6] C. Weber, "Photoacoustic CO_2-sensor for automotive applications," *Procedia Engineering*, vol. 168, pp. 3-6, Sep. 2016.

[7] R. Moolat, Manoj Mani, A. P. Viswanathan, and Mohanan Pezholil, "Compact microwave sensor for monitoring aging of oil and fuel adulteration," vol. 32, no. 5, p. e23095, Jan. 2022.

[8] C. Lopatin, "Aerospace applications of optical fiber mechanical sensors," *Opto-Mechanical Fiber Optic Sensors*, pp. 237-262, Feb. 2018.

[9] X. Lv, J. Jiang, H. Wang, Q. Gao, S. Zhao, N. Li, J. Yang, S. Wang, W. Bao, and R. Chen, "Sensitivity-compensated micro-pressure flexible sensor for aerospace vehicle," *Sensors*, vol. 19, no. 1, pp. 72, Jan. 2019.

[10] A. N. S. Javanshir, "Optical temperature sensor with micro ring resonator and graphene to reach high sensitivity," *Optik*, vol. 180, pp. 442-446, Feb. 2019.

[11] F. Zhang, Y. Zang, D. Huang, C. A. Di, and D. Zhu, "Flexible and self-powered T-pressure dual-parameter sensors using microstructure-frame-supported organic thermoelectric materials," *Nat. Commun.*, vol. 6, p. 8356, Sep. 2015.

[12] J. Wu, Z. Wu, H. Xu, Q. Wu, C. Liu, B. Yang, X. Gui, X. Xie, K. Tao, Y. Shen, J. Miaod, and L. K. Norford, "An intrinsically stretchable humidity sensor based on anti-drying, self-healing and transparent organohydrogels," *Mater. Horiz.*, vol. 7, no. 7, p. 1919, July 2020.

[13] T. Li, L. Li, H. Sun, Y. Xu, X. Wang, H. Luo, Z. Liu, and T. Zhang, "Humidity sensors: Porous ionic membrane based flexible humidity sensor and its multifunctional applications," *Adv. Sci.*, vol. 4, no. 5, p. 1600404, May 2017.

[14] S. Xiao, J. Nie, R. Tan, X. Duan, J. Ma, Q. Li, and T. Wang, "Fast-response ionogel humidity sensor for real-time monitoring of breathing rate," *Mater. Chem. Front.*, vol. 3, no. 3, pp. 484-491, Mar. 2019.

[15] S. Gong, W. Schwalb, Y. Wang, Y. Chen, Y. Tang, J. Si, B. Shirinzadeh, and W. Cheng, "A wearable and highly sensitive pressure sensor with ultrathin gold nanowires," *Nat. Commun.*, vol. 5, p. 3132, Feb. 2014.

[16] S. C. B. Mannsfeld, B. C.-K. Tee, R. M. Stoltenberg, C. V. H.-H. Chen, S. Barman, B. V. O. Muir, A. N. Sokolov, C. Reese, and Z. Bao, "Highly sensitive flexible pressure sensors with microstructured rubber dielectric layers," *Nat. Mater.*, vol. 9, no. 10, pp. 859-864, Sep. 2010.

[17] E. Amin, M. Karmakar, and B. Jensen, "Fully printable chipless RFID multi-parameter sensor," *Sens. Actuat. A-Phys.*, *A. Physical*, vol. 248, pp. 223-232, Sep. 2016.

[18] L. Dong, L. F. Wang, and Q. A. Huang, "Implementation of multiparameter monitoring by an LC-type passive wireless sensor through specific winding stacked inductors," *IEEE Internet of Things J.*, vol. 2, no. 2, pp. 168-174, Apr. 2015.

[19] Z. Abbasi, P. Shariaty, M. Nosrati, Z. Hashisho, and M. Daneshmand, "Dual-band microwave circuits for selective binary gas sensing system," *IEEE T. Microw. Theory*, vol. 67, no. 10, pp. 4206-4219, Oct. 2019.

[20] L. Ali, C. Wang, F. Y. Meng, K. Adhikari, Y. Wei, J. Li, Z. Song, and M. Zhao, "Design and optimization of interdigitated microwave sensor for multidimensional sensitive characterization of solid materials," *IEEE Sens. J.*, vol. 21, no. 20, pp. 22814-22822, Oct. 2021.

[21] Y. Zhao, X. Zhao, Q. Zuo, Y. Guo, H. Huang, H. Zhang, T. Wang, N. Wen, H. Chen, T. Cong, J. Muhammad, X. Yang, X. Wang, Z. Fan, and L. Pan, "Structural engineering of hierarchical aerogels comprised of multi-dimensional gradient carbon nanoarchitectures for highly efficient microwave absorption," *Nano-Micro Lett.*, vol. 13, no. 1, p. 144, Dec. 2021.

[22] M. Saadat-Safa, V. Nayyeri, M. Khanjarian, M. Soleimani, and O. M. Ramahi, "A CSRR-based sensor for full characterization of magneto-dielectric materials," *IEEE T. Microw. Theory*, vol. 67, no. 2, pp. 806-814, Feb. 2019.

[23] N. Javanbakht, G. Xiao, and R. E. Amaya, "Portable microwave sensor based on frequency-selective surface for grain moisture content monitoring," *IEEE Sensors Letters*, vol. 5, no. 11, pp. 1-4, Nov. 2021.

[24] Y. H. Cao, K. Chen, C. Ruan, and X. Zhang, "Robust and sensitive metamaterial-inspired microfluidic sensor for liquids with low dielectric constants," *Sensor Actuat. A-Phys.*, vol. 331, p. 112869, Nov. 2021.

[25] E. Rahamim, D. Rotshild, and A. Abramovich, "Performance enhancement of reconfigurable metamaterial reflector antenna by decreasing the absorption of the reflected beam," *Appl. Sci.-Basel*, vol. 11, no. 19, p. 8999, Oct. 2021.

[26] Q. Liu, Y. F. Yu, W. S. Zhao, and H. Li, "Microfluidic T sensor based on T-dependent dielectric property of liquid," *Chinese Phys. B*, vol. 29, no. 1, p. 10701, Jan. 2020.

[27] E. M. Amin and N. C. Karmakar. "Development of a low cost printable humidity sensor for chipless RFID technology," in *2012 IEEE International Conference on RFID-TA*, pp. 165-170, Nov. 2012.

[28] H. Lobato-Morales, A. Corona-Chávez, J. L. Olvera-Cervantes, R. A. Chávez-Pérez, and J. L. Medina-Monroy, "Wireless sensing of complex dielectric permittivity of liquids based on the RFID," *IEEE T. Microw. Theory*, vol. 62, no. 9, pp. 2160-2167, Sep. 2014.

[29] A. K. Jha, N. Delmonte, A. Lamecki, M. Mrozowski, and M. Bozzi, "Novel MNZ-type microwave sensor for testing magnetodielectric materials," *Sci. Rep.*, vol. 10, no. 1, p. 16985, Oct. 2020.

[30] Z. Zhou, Y. Li, H. Li, W. Sun, I. Liberal, and N. Engheta, "Substrate-integrated photonic doping for near-zero-index devices," *Nat. Commun.*, vol. 10, no. 1, p. 4132, Sep. 2019.

[31] V. Pacheco-Peña, M. Beruete, P. Rodríguez-Ulibarri, and N. Engheta, "On the performance of an ENZ-based sensor using transmission line theory and effective medium approach," *New J. Phys.*, vol. 21, p. 043056, Apr. 2019.

[32] I. Liberal, A. M. Mahmoud, Y. Li, B. Edwards, and N. Engheta, "Photonic doping of epsilon-near-zero media," *Sci.*, vol. 355, no. 6329, pp. 1058-1062, Mar. 2017.

[33] Q. Deng. "A BP neural network optimisation method based on dynamical regularization," *Journal of Control and Decision*, vol. 6, no. 2, pp. 111-121, Jan. 2018.

[34] C. Wang, X. Liu, L. Gan, and Q. Cai, "A dual-band non-destructive dielectric measurement

sensor based on complementary split-ring resonator," *Front. Phys*., vol. 9, p. 669707, Apr. 2021.
[35] K. T. Muhammed Shafi, J. Abhishek Kumar, and M. Jaleel Akhtar, "Dual band RF sensor for testing of magnetic properties of materials using meandered line SRR," *Sens. Actuat. A*, vol. 272, pp. 170-177, Apr. 2018.
[36] W. N. Liu, J. J. Zhang, and K. M. Huang, "Dual-band microwave sensor based on planar rectangular cavity loaded with pairs of improved resonator for differential sensing applications," *IEEE T. Instrument*, vol. 70, pp. 1-8, Nov. 2021.
[37] M. A. H. Ansari, A. K. Jha, and M. J. Akhtar, "Dual band microwave sensor for dielectric characterization of dispersive materials," in *Asia-Pacific Microwave Conference IEEE*, vol. 1, pp. 1-3, Dec. 2015.
[38] F. Requena, N. Barbot, D. Kaddour, and E. Perret, "Chipless RFID temperature and humidity sensing," in *2021 IEEE MTT-S International Microwave Symposium (IMS)*, pp. 545-548, June 2021.

Qiao Yu Li is currently pursuing the doctor's degree of Electromagnetic Field and Microwave Technology in Shanghai University, Shanghai 200444, China. She received the B.S. degree in Engineering from Henan normal University, Xinxiang, China, in 2016, received the master's degree in Electromagnetic Field and Microwave Technology from Shanghai University, Shanghai 200444, China, in 2019. Her current research is focused on plasmonic sensor devices.

Yu Wei Mao received the B.S. degree from Bengbu College, Bengbu, China, in 2015, obtained the master's degree in Communication and Information Engineering at Shanghai University, Shanghai 200444, China, in 2018. Her current research is focused on near-zero medium sensor technology.

Yong Jin Zhou received the B.S. degree in communication engineering from Shandong University, Jinan, China, in 2006, and Ph.D. degree in electromagnetic field and microwave technology from Southeast University, Nanjing, China, in 2011. From 2009 to 2010, he was a visiting scholar of University of Houston. From 2011 to 2012, he was a software engineer with EEBU of Marvell Technology (Shanghai) Ltd. From 2012 to 2015, he was an Assistant Professor with School of Communication & Information Engineering, Shanghai University, Shanghai, China. From 2015, he was an Associate Professor with School of Communication & Information Engineering, Shanghai University, Shanghai, China. From 2020, he was a Professor with School of Communication & Information Engineering, Shanghai University, Shanghai, China. His current research interests include plasmonic metamaterials, millimeter wave and THz functional devices, wireless energy transmission, and computational electromagnetism. He has served as *Applied Computational Electromagnetics Society (ACES) Journal* guest editor and is serving as a Youth Editorial Board Member *Journal of Electronics & Information Technology*. He is serving as a Reviewer for over 20 peer-reviewed journals, such as *Nature Electronics, Photonic Research, Optics Letter, Optics Express, Appl. Phys. Express, IEEE Access, IEEE MTT, IEEE MWCL*. He has served as a session chair for several International Symposiums.